Strong Higgs binding of heavy-fermion systems

Pankaj Jain,[a] Alan J. Sommerer,[b] Douglas W. McKay,[a] J. R. Spence,[b] J. P. Vary,[b] and Bing-Lin Young[b]
[a]*Department of Physics and Astronomy, The University of Kansas, Lawrence, Kansas 66045-2151*
[b]*Department of Physics and Astronomy and Ames Laboratory, Iowa State University, Ames, Iowa 50011*
(Received 27 May 1992)

We study the fermion-antifermion bound-state spectrum for heavy quarks and leptons by including the effect of Higgs-boson exchange. We use the Bethe-Salpeter equation in the ladder approximation and the N/D method for our calculation. The ladder Bethe-Salpeter equation is solved by using several well-known approximation schemes: the instantaneous approximation, the Blankenbecler-Sugar approximation, and covariant expansion in terms of Tschebeshev polynomials. Our results show that for quark-antiquark systems the Higgs-boson exchange generally dominates over QCD for quark masses larger than 500 GeV, and leads to very deep binding for quark masses in the TeV region. In the absence of the QCD force, as is the case with leptons, we determine the minimum value of the fermion mass needed to form a bound state as a function of the Higgs-boson mass. We further find that tightly bound states where the bound-state masses drop to zero appear for fermion masses between 1 and 1.8 TeV for all the approximations to the Bethe-Salpeter equation that we employed. The N/D method also leads to tightly bound states for fermion masses larger than about 1 TeV but does not in general yield zero-mass bound states. The meaning of the tightly bound states is discussed.

PACS number(s): 14.80.Gt, 11.10.St, 11.50.Ec, 12.38.Lg

I. INTRODUCTION

The standard model of $SU_C(3)\times SU_L(2)\times U(1)$ interactions with a fundamental scalar boson sector has the interesting property that the fermion Yukawa coupling, which takes the form $g_Y=m_f/v$, where m_f is the fermion mass and $v\cong 250$ GeV is the electroweak symmetry-breaking energy scale, increases with the fermion mass. The quark-quark interaction, which is dominated by color $SU_C(3)$ gluon forces for quarks of mass up to a few hundreds of GeV, will be subject to a significant scalar force due to Higgs-particle exchange when the quark mass further increases. The Higgs-boson-exchange force will eventually become dominant as the quark mass rises to more than approximately 500 GeV. The Higgs particle effects are larger the lighter its mass, of course, and multiscalar multiplet models can also complicate the picture. But the general feature that *some* Higgs particle exchange force will get strong as fermion masses get large should survive the model-dependent details.

The feature of the Yukawa coupling mentioned above is academic for the experimentally confirmed quarks because their masses are small in comparison with the electroweak symmetry-breaking scale v. The experimental lower bound on the mass of the top quark, m_t, is now 91 GeV [1], and, within the minimal standard model framework, experimental data constrain m_t to be in the vicinity of 150 GeV [2]. Given such a high value of the lower bound of m_t, for which the Higgs-boson effect can no longer be discarded, and the possibility of even heavier fermion mass scales associated with supersymmetry or a possible nearly degenerate fourth generation, for example—the interest in probing the effects due to Higgs-boson exchange in heavy fermion systems is far from academic. Furthermore, it is possible that very heavy neutrinos exist that have no electric or color charge yet are able to form bound states through the Yukawa coupling.

The study of heavy fermion interactions within the standard model framework dates back some time. Unitarity constraints on the scattering amplitudes [3] and radiative correction effects on low-energy processes [4] have been used to constrain Higgs particle and fermion masses in the standard model. In the past few years, several studies using the Schrödinger equation have focused on the Higgs-boson effects in ultra-heavy-fermion–antifermion bound states [5–7]. In a related topic, several authors [8–10] have elaborated on the theoretical study of the $\bar{t}t$ threshold region by Fadin and Khoze [11] to include QCD effects more completely [9,10] and to include Higgs-boson-exchange effects [8,9]. Both Refs. [8] and [9] use a Yukawa potential in a nonrelativistic approximation and conclude that for $m_t > 150$ GeV the Higgs-boson exchange can affect the cross section significantly enough to complicate the interpretation of the threshold behavior.

We report here on the results of studying heavy quark binding subject to the gluon and Higgs-boson-exchange interactions, using the field-theoretical Bethe-Salpeter (BS) equation. We focus on the bound-state problem in the strong-coupling regime. Several widely used schemes of treating the kernel of the ladder approximation are adopted. We report their predictions for the binding energies of low-lying states as functions of $\alpha_{\rm QCD}$, m_f, and the Higgs-boson mass M_H. Although the computational tools for dealing with the strong binding are not well established, the topic of deep binding and therefore large coupling in the BS equation has been studied by a number of authors in relation to analytic solutions of the BS

equation [12]. Our motivation is different. Our viewpoint is that the ladder BS equation, which partially sums up the perturbative series, represents a scheme of approximation which allows us to examine some of the main features of the strong binding problem at intermediate couplings. Such an approximation, like all approximations, will break down eventually, and hence our study will allow us to find out where the approximation ceases to make sense or when new physics may emerge and has to be examined in a more appropriate framework.

It is expected that for heavy quarks the confining force contributes very little to the bound-state energy. The bound-state characteristics can be attributed to the Coulombic gluon interaction and, in our consideration, the Higgs-boson interaction. In order to see the effect of this interaction and its interplay with the gluon interaction, we will study the pure Higgs-boson interaction first and then combine it with the QCD interactions to study the total binding force of the standard model. We will employ four known approximations to the BS equation for these studies: (a) the instantaneous approximation including both the positive- and negative-frequency parts of the amplitude, denoted as IA1; (b) the instantaneous approximation with the positive-frequency part of the amplitude only, denoted as IA2; (c) the covariant gauge ladder (CGL) approximation; and (d) the Blankenbecler and Sugar (BBS) approximation. For comparison we also consider the Schrödinger equation and the N/D method. The latter is a dynamic scheme which unitarizes the t-channel Born diagram of a scattering amplitude. It generates not only a right-handed cut but also bound-state poles if the t-channel exchange represents an attractive force. Therefore the N/D method is also an appropriate scheme for the study of the strong binding problem.

In Sec. II we study the effect of the pure scalar exchange, ignoring the confinement and one-gluon-exchange effects. As in the nonrelativistic potential model [5], we find that in all the BS schemes we have considered, a pure Higgs-boson-exchange force supports bound states only when the Yukawa coupling $g_Y \propto m_f/v$, or the fermion mass, is greater than a critical value which depends on M_H. We find that the mass of the bound state increases with the fermion mass at first. In the deep binding limit, the bound-state mass drops to zero, and in some approximation schemes, rather abruptly. We refer to the coupling value at which the bound-state mass goes to zero as the "collapsing coupling."

For comparison, we include in Sec. III a study of the strong binding limit of the various ladder approximation schemes in the pure "QED gluon" case. As expected from previous studies [13], the ground-state ($J^P=0^-$) mass of the bound state goes to zero as the coupling increases, sometimes rather abruptly depending on the approximation being used. The collapsing coupling is smaller than that of the Yukawa interaction in the corresponding cases. We compare the numerical results of the different models of the Bethe-Salpeter kernel to each other and to the weak-coupling expansion in the literature on the positronium spectrum.

In Sec. IV we investigate the bound-state problem by combining the QCD interaction with the Higgs-boson-exchange force. A brief discussion is given in Sec. V, where we also discuss the effect of the Z^0 contribution, in particular its longitudinal component whose effects we found in general to be small in the weak- and intermediate-coupling regions where a perturbative kernel is appropriate. Some details of the BS equation in the previous approximations employed in this article are given in Appendix A. The N/D method applied to a scalar exchange is given in Appendix B. Throughout this work only the ground state of the fermion-antifermion system is considered for illustration, though several remarks on vector-meson bound states are included in Appendix A. The behavior of the excited states will be considered in a later work.

II. SCALAR BOSON EXCHANGE: THE HIGGS-BOSON EFFECT

Scalar-meson exchange generates an attractive force in fermion-fermion and fermion-antifermion systems, and it was established long ago that a significant scalar exchange contribution is needed to account for low-energy nucleon-nucleon scattering data in particle exchange models of the strong interaction [14]. Curiously enough, the weak interaction sector of the standard model with fundamental scalar fields and heavy fermions ($\sim 10^3 \times$ mass of nucleon) contains a strong-coupling fermion-scalar meson sector with Yukawa coupling $g_Y \sim m_f/v \geq 4$. It is natural to explore this strong-coupling situation, and in this section we report the results of relativistic bound-state calculations with a Higgs-boson-exchange kernel which is essentially the whole story in the heavy neutrino and heavy lepton cases. We note that the forces arising from scalar exchanges for the fermion-fermion and fermion-antifermion systems are of the same sign. This can be understood from the fact that the scalar interaction is like a mass term.

For orientation, we first summarize the result of a Schrödinger equation analysis of the problem, with a Yukawa potential modeling the Higgs-boson-exchange effect as given in Ref. [5]. Using a variational argument, one finds the condition for the existence of a bound state of the $f\bar{f}$ system to be [5]

$$G_F m_f^3 > 4\sqrt{2}\pi M_H \ , \tag{1}$$

where G_F is the Fermi constant. Equation (1) provides a useful guideline for the region where Higgs-boson exchange is expected to dominate. However, the field-theoretical approach becomes essential when the fermion mass m_f is of the order of hundreds of GeV. We need a more complete formalism to assess the Higgs particle binding effects.

We adopt the ladder approximation to the BS equation. We evaluate the energy of the ground-state $f\bar{f}$ system using both the covariant kernel

$$K(q) = g_Y^2 \frac{1}{q^2 - M_H^2} \ , \tag{2a}$$

which is used in the covariant gauge ladder approxima-

tion, and the instantaneous approximation to this kernel,

$$K(|\mathbf{q}|^2) = -g_Y^2 \frac{1}{|\mathbf{q}|^2 + M_H^2} \ . \tag{2b}$$

The instantaneous approximation simplifies the problem to a three-dimensional one where the BS amplitude can be readily integrated over the time component of the four-momentum to yield Salpeter's equations. In the evaluation of Salpeter's equations, one can take into account both the positive- and the negative-frequency parts of the wave function or simply the positive-frequency part. They are, respectively, the approximation schemes denoted as IA1 and IA2. See Appendix A 2 for a summary of these methods.

Another three-dimensional reduction of the BS equation that we have used is the Blankenbecler-Sugar equation. The Blankenbecler-Sugar scheme replaces the two free fermion propagators appearing in the BS equation with an appropriately chosen substitute propagator. The substitute propagator is chosen to contain the correct imaginary part of the nonrelativistic propagator, to preserve elastic unitarity, and to allow reduction of the BS equation to a Lippmann-Schwinger-type equation. The Blankenbecler-Sugar propagator contains positive-energy projection operators so that only positive-energy components of the wave functions appear, and it contains a δ function that accomplishes the reduction to three dimensions. Like the instantaneous approximation, the Blankenbecler-Sugar equation ignores boson retardation. See Appendix A 3 and references therein. The instantaneous approximation and the Blankenbecler reduction are the classic first approximations to the kernel for positronium studies [15,16].

The calculation of the ground-state binding energy in the Feynman gauge CGL approximation is sketched in Appendix A 4.

The minimum fermion mass (minimum Yukawa coupling) m_f^0 at which bound states begin to form is shown in Fig. 1 as a function of M_H. Also shown is the corresponding Schrödinger equation result of Eq. (1), and the result of an N/D model analysis. The Yukawa coupling is taken to be the standard model form, $g_Y = m_f/250$ GeV. We do not include momentum dependence of this coupling in the calculations presented here, since we are exploring the general features of strong binding without attempting detailed numerical predictions. The questions of the choice of mass scale for evaluating the couplings and the possible strong momentum dependence at the largest fermion masses considered are discussed in Appendix A 2. The minimum fermion mass, i.e., minimum Yukawa coupling, necessary for binding to occur increases with the Higgs-boson mass. Experimental studies at the CERN e^+e^- collider LEP now put a lower bound on the standard Higgs-boson mass at 50 GeV, which limits the strength of the Higgs effects for a given fermion mass according to Fig. 1. In order for the binding to occur by the Higgs-boson-exchange force alone, the fermion mass cannot be less than about 400 GeV.

Comparing the various formalisms we see that they all give qualitatively similar results. With the exception of the CGL approximation for $M_H > 180$ GeV, the field-theoretical schemes bind lighter fermions for a given Higgs mass than does the Schrödinger equation result. In the N/D calculation the subtraction point s^0 in Eq. (B7) or R_0^2 in Eq. (B8a) is taken to be zero. We choose this particular value for the subtraction by requiring that the N/D curve pass through the origin, the one point common to all other curves.

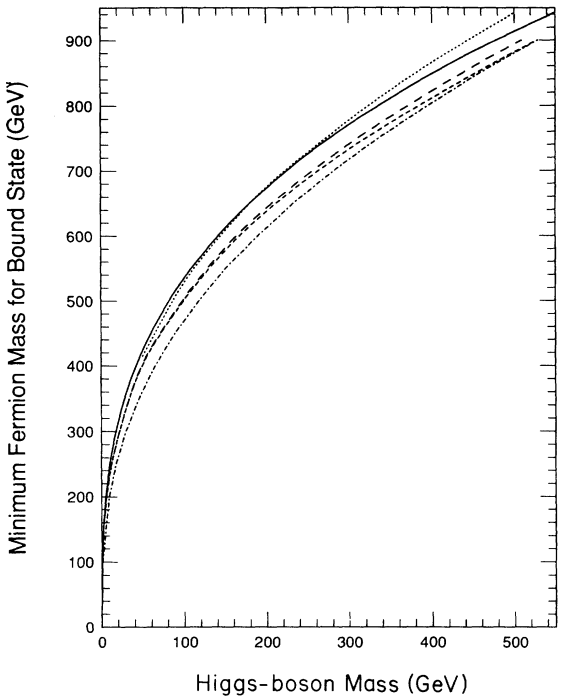

FIG. 1. Minimum fermion mass for which a fermion-antifermion bound state can form when the fermions interact solely through the exchange of a Higgs scalar of a given mass. Solid curve: variational Schrödinger solution; dotted curve: CGL; long dash curve: IA1 and IA2; short dash curve: BBS, dash-dot curve: N/D.

For a top quark with $m_t \leq 150$ GeV, the Higgs effects are small for $M_H > 50$ GeV, not yet comparable to the QCD Coulomb energy, as already noted in several papers [8,9]. It is therefore interesting to examine the case of heavier fermions. Increasing the fermion mass pushes the Higgs interaction to the "deep-binding" region where it becomes the dominant fermion binding force. If the fermion mass is large enough, the system becomes so tightly bound that its invariant mass is zero; that is, the binding energy is $2m_f$. The fermion mass at which the bound-state mass goes to zero and how fast the bound-state mass falls to zero with increasing fermion mass depends on the formalism used. One purpose of this study is to establish a mass scale beyond which the bound-state formulations which we use cease to be valid and we take this as the energy scale where different physics may emerge. We will come back to this point in the discussion section.

Our calculations should, however, be qualitatively reliable in the intermediate-coupling region where the binding energy is much larger than that provided by QCD but still small compared to twice the fermion mass. They

suggest the exciting possibility of a region where rather tightly bound, ultraheavy systems exist. Depending on its actual mass value, which will affect the available decay channels of the bound states, it may be long lived.

In Fig. 2 we show for six different models the ground-state mass as a function of the fermion mass, $g_Y = m_f/250$ GeV, as in the standard model. We note that the full propagator CGL, BS equation, and N/D models are fully covariant; the Blankenbecler-Sugar equation and the instantaneous approximations include some relativistic effects. Solutions to the Schrödinger equation with Yukawa potential, which is not expected to be applicable in the deep binding region, are shown for comparison purposes. In the four BS schemes we show two curves each to exhibit the variation arising from different choices of the Higgs-boson mass. The upper and lower curves are, respectively, for $M_H = 200$ and 50 GeV. The single curve for the Schrödinger and N/D are for $M_H = 100$ GeV.

From Fig. 2 we see that for $m_f < 1$ TeV all formulations under consideration give bound-state masses which continue to rise with m_f. Up to moderate coupling values, $m_f < 600$ GeV, results of various schemes are similar although not identical. It is interesting to note that the Schrödinger equation lies in the middle of the various relativistic results, below CGL and IA2 approximations but above BBS and IA1 approximations. For $m_f \approx 1.8$ TeV, the bound-state energy vanishes in all the formulations except for the N/D approach. Taking the curves literally, we would conclude that there is no $m_f > 1.8$ TeV possible when the fermion is subject to a Yukawa coupling of the spontaneous symmetry-breaking type.

The drastically different behavior of the N/D approach as shown in Fig. 2 at large Yukawa coupling requires some explanation. The bound-state energy actually goes to zero asymptotically for $m_f \to \infty$ for our choice of $s_0 = 0$. The mechanics of this result can be readily seen from Eq. (B7). The integral is non-negative for the spectral function as given in Eq. (B6). In order for the equation to be satisfied, we have to have

$$s_B \geq s_0 \ , \tag{3}$$

and $s_B \to 0$ only for $m_f \to \infty$, where s_B is the bound-state mass squared. The subtraction, which in general is necessary to render the dispersion integral convergent, effectively introduces, in the present consideration, a repulsive core to cancel some of the effect of the attractive force. Depending on the value chosen for s_0, the bound-state energy may not vanish even for $m_f \to \infty$. If the subtraction scheme for rendering the integral convergent has any validity, it shows that collapse of the bound-state system will not necessarily occur even for infinite couplings.

For completeness we also investigate the effect of varying the Yukawa coupling for fixed fermion and Higgs-boson masses. We show in Fig. 3 a graph of bound-state mass vs the strength of the Yukawa coupling, α_Y, again in the absence of other forces, for fermion masses of 150, 500, and 1000 GeV and Higgs mass $M_H = 100$ GeV. All three curves are IA1 results. These curves are appropriate for a model where the Yukawa coupling of the fermion to the scalar is *independent* of the fermion mass, unlike the case of the standard model. There are several interesting features of this type of coupling. (a) For given

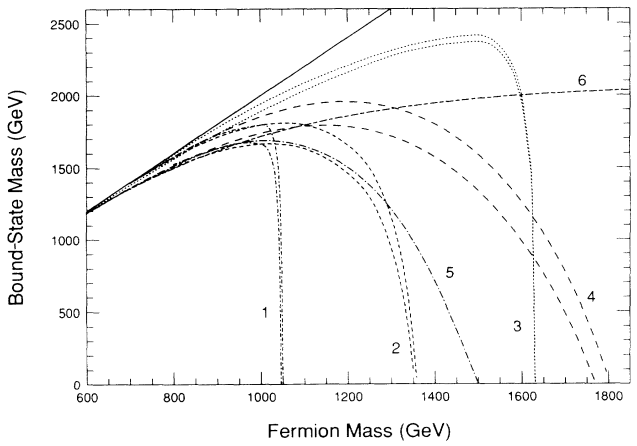

FIG. 2. Ground-state (0^-) bound-state mass of fermion-antifermion system vs fermion mass when the fermions interact solely through exchange of a massive Higgs scalar. Solid line: $M_B = 2m_f$ line, the "edge" of the continuum; pair 1: IA1; pair 2: BBS; pair 3: CGL; pair 4: IA2; for each pair the upper curve was computed with $M_H = 200$ GeV, the lower with $M_H = 50$ GeV. Curve 5: variational Schrödinger equation solution; curve 6: N/D. A Higgs-boson mass of 100 GeV was used in computing curves 5 and 6.

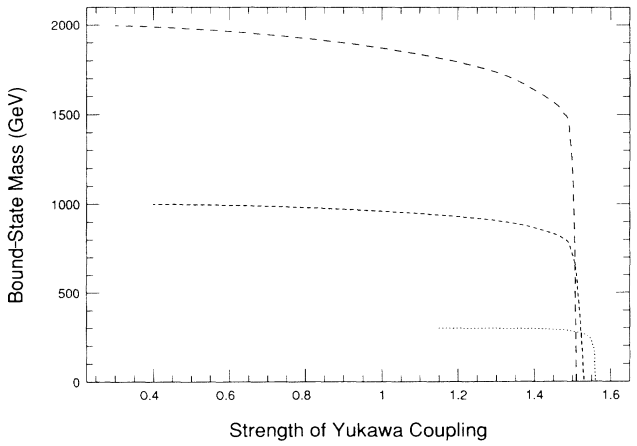

FIG. 3. Ground-state (0^-) mass of a fermion-antifermion bound state in which the fermions interact solely through the exchange of a massive scalar boson, shown for three different fermion masses vs the coupling strength of the interaction. Dotted curve: $m_f = 150$ GeV; short dash curve: $m_f = 500$ GeV; long dash curve: $m_f = 1000$ GeV; all curves were computed with $M_H = 100$ GeV using IA1. The horizontal axis is $g^2/4\pi$, where g is *not* proportional to the fermion mass as is the case when the scalar boson is a Higgs boson. The coupling at which each curve begins on the left is approximately the minimum coupling necessary to bind the fermions.

values of m_f and M_H there is a minimal coupling strength for the binding to occur. This is similar to the effect shown in Fig. 1. The value of the coupling at the left end of the curves indicates this minimal coupling for each of the fermion masses considered. (b) The minimal coupling decreases as the fermion mass increases. This shows that the scalar interaction is more effective in forming bound states for heavy fermions. (c) For a fixed scalar mass, the collapsing coupling at which the bound-state mass vanishes has a very weak dependence on the fermion mass. As shown in Fig. 3 the collapsing coupling α_Y where the bound-state mass goes to zero varies from 1.5 to 1.6 for m_f varying from 150 to 1000 GeV. This is similar to the behavior shown in Fig. 2 for IA1, where the scalar coupling is proportional to m_f. Figure 2 shows the IA1 bound-state mass going to zero at $m_f \approx 1050$ GeV, i.e., at $\alpha_Y = 1.45$. Discussion of possible effects due to running of the Yukawa coupling is given in Appendix A 2. The point of this plot is to illustrate the fact that a new scalar interaction with $g_Y \approx 3$ can produce important, perhaps dominant, bound-state effects in the mass scale region which is of interest for the next generation of collider experiments.

III. MASSLESS VECTOR-BOSON EXCHANGE

In this section, we briefly review results of various models for bound-state formalism based on constant coupling, massless vector boson t-channel exchange. This class of models is relevant to the ground state of QED and to slowly running QCD-like theories with colorless bound states (no single gluon annihilation graphs in the 1^- channel). An extensive literature exists [17] and the predictions can be readily compared with appropriate experimental data in the weak-coupling case such as positronium. Furthermore, work on strong-coupling limits exists in some of the models. In particular, the deep-binding limit at the breakdown couplings of $M_B \to 0$ for the ground state, 0^-, and the lowest 1^- state have been investigated in the covariant gauge BS equation in Ref. [12].

We first compare the QCD one-gluon-exchange effect with that of the Higgs-boson exchange. Figure 4 shows the 0^- bound-state mass vs quark mass for a constant coupling value $\frac{4}{3}\alpha_{\rm QCD} = 0.25$ and Higgs-boson exchange with $M_H = 100$ GeV in the region around $m_f \simeq 450$ GeV, where the latter becomes dominant. The use of a momentum-independent $\alpha_{\rm QCD}$ and the choice of its effective value is discussed in Appendix A 2. The "QED-like" QCD model will be discussed further in Sec. IV. The top (solid) curve is the straight line of slope 2. The second (dotted) curve is a plot of the order-α^4 perturbative result ($E/M = 2 - \alpha^2/4 - 21\alpha^4/64$). The IA2 and BBS bound-state energies for one-gluon exchange lie essentially on top of this line over the range of quark masses covered by the figure. The IA2 result lies slightly below this line but is not shown. The third (long dash lines) curve is the IA2 and BBS result when both gluon and Higgs couplings are considered. The bottom curve gives the result of IA1. The two bottom curves both drop to zero as the quark mass increases to values beyond that

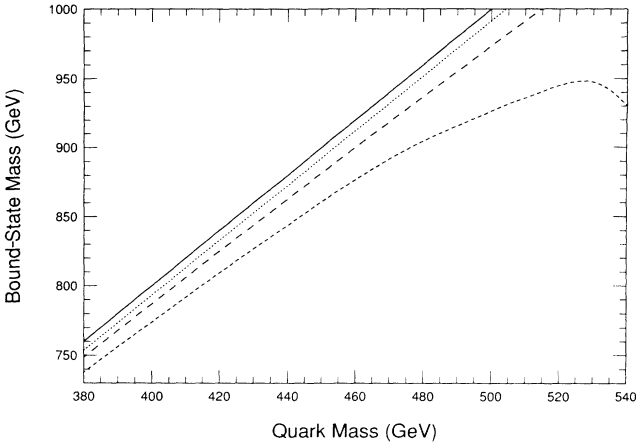

FIG. 4. Quarkonium 0^- bound-state mass vs quark mass. The quarks interact through both one-gluon exchange (OGE) and Higgs-boson exchange (HBE). Also shown for comparison is the line displaying the bound-state mass when the quarks interact solely via OGE. The OGE-only line shown also approximates closely the order-α^4 vector boson exchange result. A Higgs mass of 100 GeV was used in computing the curves. Solid line: $M_B = 2m_f$ line; dotted line: order-α^4 and one-gluon-exchange IA2 and BBS results; long dash curve: one-gluon exchange with Higgs interaction IA2 and BBS result; short dash curve: one-gluon exchange with Higgs interaction IA1 result.

covered by the figure. We will come back to them again in Sec. IV. We see from Fig. 4 that the Yukawa coupling becomes dominant above about 500 GeV for IA2 and BBS, and is already dominant at 400 GeV for IA1.

Next we study the dependence of the binding energy on the strength of the (nonrunning) massless vector boson coupling constant. In Fig. 5 plots of ground-state mass

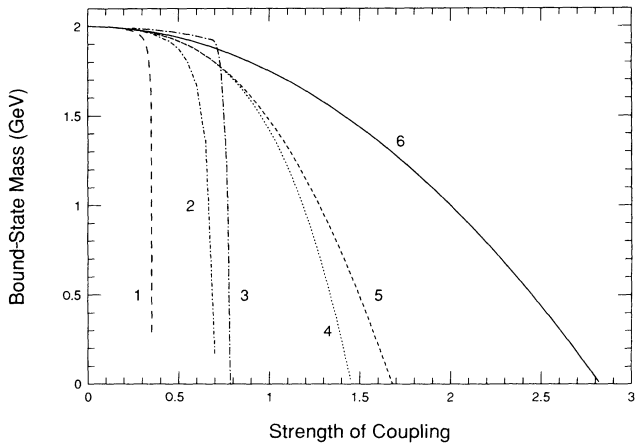

FIG. 5. Quarkonium 0^- bound-state mass vs strength of one-gluon-exchange interaction coupling. Also shown for comparison are the order-α^2 and -α^4 perturbative results. Since the bound-state mass scales with the fermion mass, the fermion mass was set at one GeV in computing the curves. Horizontal axis is $\frac{4}{3}\alpha_s$. For each curve, the binding gets stronger as the coupling increases until the bound-state mass is driven to zero. Curve 1: IA1; curve 2: IA2; curve 3: CGL; curve 4: order-α^4 result; curve 5: BBS; curve 6: order-α^2 (Schrödinger) result.

vs coupling are shown for this pure QED-like case for IA1, IA2, BBS, and CGL approximations. The order-α^2 ($E=2-\alpha^2/4$) and order-α^4 ($E=2-\alpha^2/4-21\alpha^4/64$) perturbative results [18] are also shown for comparison. Since the bound-state mass scales with the fermion mass, we set the fermion mass to unity. Clearly the IA1 method gives the steepest descent to the "deep-binding" region. This is caused primarily by the two-body velocity operator $\boldsymbol{\alpha}_1\cdot\boldsymbol{\alpha}_2$, which gives rise to large off-diagonal matrix elements between the positive- and negative-frequency wave functions (see Appendix A 2). With the exception of the BBS model, the BS models all drive the bound-state mass to zero much more quickly than the order-α^4 curve, with collapsing couplings of $0.35<\frac{4}{3}\alpha<0.8$.

As a further comparison we note that the semirelativistic reduction of a two-body Dirac formalism has been used to generate an energy eigenvalue equation for positronium good through order α^4, which can be solved exactly [19]. Plotting this bound-state eigenenergy as a function of coupling yields a curve which begins to fall rapidly toward zero as the coupling approaches 0.5. (This curve is not shown in Fig. 5; the small coupling part of it is shown in Fig. 6.) The eigenenergy becomes complex for couplings larger than 0.5 presumably indicating a breakdown of the semirelativistic reduction at large coupling.

In Fig. 6 a blowup of the weak binding region is given. The CGL and IA1 models form upper and lower boundaries of an envelope with the α^2, α^4, BBS, and IA2 approximations, and the two-body Dirac formalism falling in between. The BBS solution tracks the order α^4 curve remarkably closely all the way out to the strong-coupling limit. The CGL approximation is known to contain

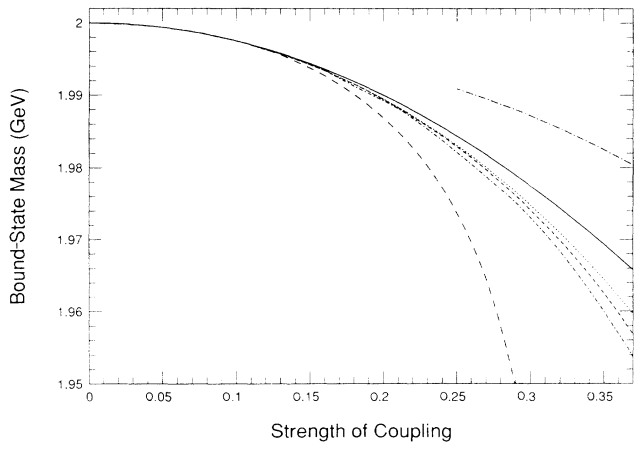

FIG. 6. A blowup of the small coupling region of Fig. 5. A curve representing the two-body Dirac formalism (see text) has been added to the figure for comparison. Since the bound-state mass scales with the fermion mass, the fermion mass was set at one GeV in computing the curves. Horizontal axis is $\frac{4}{3}\alpha_s$. Long dash-dot curve: CGL; solid curve: order-α^2 (Schrödinger) result; dotted curve: BBS and order-α^4 result; short dash curve: two-body Dirac formalism; short dash-dot curve: IA2; long dash curve: IA1.

$\alpha^3\ln\alpha^{-1}$ and α^3 terms which disagree with the positronium ground-state value [20,21]. In fact, as described in Appendix A 4, the numerical solution shown in Fig. 6 is in agreement with the $\alpha^3\ln\alpha^{-1}$ and α^3 deviations from the lowest-order α^2 Schrödinger result, confirming the reliability of the numerical procedure.

It has long been known that the radiation gauge has enormous advantages in capturing the main features of the experimental positronium spectrum and in serving as a practical gauge for doing perturbation theory refinements on the spectrum and calculations of transition rates. But how one extrapolates results to the strong-coupling, deep-binding relativistic regime is not known, and we offer the range of models shown here as an indication of the range of extrapolations one might expect. The striking feature that we wish to emphasize is that a rather abrupt transition to a deep-binding, $M_B=0$, limit occurs in the range $0.35<\frac{4}{3}\alpha<1.7$ for the various models, while in the $\alpha\to 0$ limit they converge on the leading-α^2 Schrödinger result from above and below.

IV. THE FULL STANDARD MODEL BINDING FORCES

In the preceding sections we have seen the effects of the scalar and vector binding forces separately. For the same value of coupling strength the vector interaction causes stronger binding than the scalar interaction. In this section we investigate the effect of combining the two interactions. This is the total standard model force for heavy fermions, neglecting the electroweak interaction. We will comment on the effect of the longitudinal component of the Z^0 in the next section. We take $M_H=100$ GeV, and the QCD fine structure constant to be $\frac{4}{3}\alpha_{\rm QCD}=0.25$ by ignoring the slowly running effect. Note that this coupling is nearly three-fourths the IA1 collapsing coupling for one-gluon exchange alone (see Fig. 5). The Yukawa coupling constant is the conventional form $g_Y=m_f/v$. We consider the CGL, IA1, IA2, and BBS models. The results are shown in Fig. 7. The IA2 and BBS bound-state energies are driven to zero at slightly lower quark masses than in the case where the Yukawa interaction alone was considered (see Fig. 2). The IA1 curve of Fig. 7, however, plunges to a zero mass at a much smaller quark mass than the Higgs-boson-exchange-only result of Fig. 2. Without the gluon interaction, the collapsing coupling for the Yukawa interaction corresponds to a fermion mass of slightly more than 1 TeV. With the one-gluon exchange included, the collapsing coupling is significantly reduced, taking place at about $m_f=580$ GeV, almost a factor 2 smaller. We attribute this peculiarity of the IA1 curve of Fig. 7 to the fact that, as noted above, the one-gluon coupling employed in generating the curves of Fig. 7 is already close to the IA1 collapsing coupling for one-gluon exchange. In this situation the gluon contributions obviously can no longer be regarded as a perturbation even to the large coupling scalar interaction.

The momentum space wave functions and their Fourier transforms for the bound states represented in Fig. 7 were also obtained. They show that as the quark mass increases and the binding gets stronger due to larger

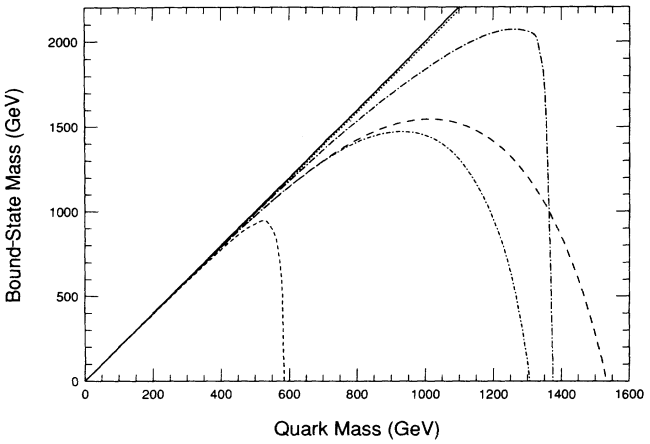

FIG. 7. Quarkonium 0^- bound-state mass vs quark mass. The quarks interact through both one-gluon exchange (OGE) and Higgs-boson exchange (HBE). Also shown for comparison is the line displaying the bound-state mass when the quarks interact solely via OGE. A Higgs mass of 100 GeV was used in computing the curves. In each case, $\frac{4}{3}\alpha_s = 0.25$ was used for the OGE coupling. Solid line: $M_B = 2m_f$ line; dotted line: IA2 and BBS result for one-gluon-exchange interaction only; long dash curve: IA2 result for one-gluon exchange with Higgs interaction; short dash-dot curve: BBS result for one-gluon exchange with Higgs interaction; short dash curve: IA1 result for one-gluon exchange with Higgs interaction; long-dash-dot curve: CGL.

scalar coupling, the rms value of the momentum grows larger while the rms radius of the spatial wave functions gets smaller. The rms radius changes most dramatically as the collapsing coupling is approached. The wave functions indicate that as the bound-state mass is driven to zero by the increasing coupling the bound state shrinks rapidly in spatial extent.

V. DISCUSSION

We have investigated in this article strong-coupling effects of the scalar force due to massive scalar particle exchange and the vector force due to massless vector boson exchange. We found that for the same coupling strength, an attractive vector exchange force is more effective in forming bound states than an attractive Yukawa force. A manifestation of this property is the existence of a minimal coupling in the case of pure scalar exchange for a given M_H, below which bound states cannot be formed. Because of the nature of the spontaneous symmetry breakdown, for light quark system where the Yukawa coupling strength is small, the QCD force is the dominant component of the binding force. The Higgs-boson-exchange effect is negligible in all the known quark sectors—even as heavy as the Υ system. However, for heavy quarks with a mass of 500 GeV or greater, the Yukawa force becomes dominant.

Realizing that the strong-coupling regime is uncharted territory, we employed several well-known bound-state calculation schemes in the hope of obtaining some valid qualitative features of the strong-coupling problem. One aspect of the present study is the appearance of bound states of zero mass. The investigation of such ultratightly bound states in the BS equation can be traced back four decades [22]. The motivation of this early study was to investigate analytic solutions of the BS ladder approximation. Physical interpretations and possibilities to avoid collapsing were offered in several later studies. For example, Haymaker [23] studied bound states in the O(N) σ model and interpreted the appearance of the tachyon solution as an indication of phase transition analogous to the transition from the symmetric phase to the symmetry-breaking phase of the Higgs potential as the Higgs mass squared varies from positive to negative values. The unphysical tachyon does not really appear in the physically accessible sheet. Caussignac and Wanders [24], working effectively in the ϕ^3 theory, found that collapsing can be avoided when a nontrivial spectral function is introduced to modify the free scalar particle propagator which enters in the ladders of the BS equation. More recently, Rupp [25] interpreted the collapsing of the scalar particle bound state in the spontaneous symmetry-breaking phase of the ϕ^4 theory as a breakdown of the vacuum [26].

The relationship of these interpretations to our work is not clear, although they are not necessarily excluded by our results. Our particle content is different and we start with a theory in which the vacuum is already broken spontaneously. We do not see how to break the vacuum further to avoid collapsing unless there emerges an energy scale which is much larger than the standard model symmetry-breaking scale, $v = 250$ GeV, so that the effective Yukawa couplings for very massive fermions are reduced. As for the modifications of the fermion propagator, the proper way to include dynamical effects is by simultaneous solutions of the Schwinger-Dyson equation for the propagator in an approximation consistent with the one used for the Bethe-Salpeter equation. Modeling of the momentum dependence of the couplings, discussed in Appendix A 2, would be appropriate at this stage of the calculation. Such a study goes beyond the goals of the present work.

There are several possibilities to interpret the collapsing of the bound state in the present study. One possibility is that the standard model still defines the group structure of the theory but a nonperturbative regime is entered beyond a certain heavy fermion mass threshold so that the perturbatively motivated approximation to the BS equation is no longer valid. Another is that the heavy fermions of TeV scale are associated with a higher symmetry-breaking scale where the heavy fermion Yukawa coupling is reduced and a perturbative treatment is still valid. Or, for a more drastic possibility, the Higgs-boson and/or the heavy fermion states are composite objects so that their couplings are softened by form factors and are much weaker than that expected from point particles. In all these possibilities, except for the first one, new physics is required when fermion mass scales of the order of 1 TeV appear.

Despite the absence of a clear interpretation of bound-state collapsing toward zero mass, we think that their occurrence is perhaps not surprising given the bound-state

equation we used. However, that the collapsing takes place in the region around 1 to 2 TeV in all the diverse approximation schemes of the BS equation, as indicated in plots of Figs. 2 and 7, is noteworthy. If the collapsing of bound state is an indication of the onset of new physics, the energy range that collapse occurs agrees with the various other estimates of the energy scale at which the standard model is expected to break down. We surmize that the region below the turnover to collapsing which is the intermediate-coupling region, the ladder approximation of the BS equation, provides a reasonably reliable description of bound-state physics. In this intermediate-coupling region the binding is already tight. The binding energy of the bound state can be a sizable fraction of the total mass of the constituents. This is a new regime of the bound-state physics. It represents an intriguing new effect to be searched for in the future collider experiments. One possibility is the formation of tight binding and strongly interacting leptonic systems if heavy leptons exist in the scheme of the standard model spontaneous symmetry breakdown. Some phenomenological studies related to this tight-binding problem, in the nonrelativistic Schrödinger approximation, have been reported in the literature [5–7], and we plan to explore experimental implications of these states in a future study.

In our investigation we have neglected the electroweak interaction, in particular the contribution of the longitudinal Z^0. At the energy regime of our consideration, one can argue that the longitudinal Z^0 effect is equivalent to that of a 0^-, Goldstone boson and hence it may not be negligible. We investigated the longitudinal Z^0 effect in the Feynman gauge. The effect of Z^0 itself in this gauge is very small. The main effect comes from the Goldstone boson which has a pseudoscalar coupling of the same magnitude as the Higgs-boson coupling, and hence increases with the mass of the fermion under consideration. Our explicit calculation in IA1, CGL, and BBS approximations shows that the inclusion of such a repulsive, pseudoscalar force decreases the binding only slightly in the intermediate-coupling region. The fact that the pseudoscalar coupling effect is not large when the bound state is not ultrarelativistic can be understood from the following consideration. The γ_5 coupling mixes the large and small components of the fermion spinor wave function and the coupling vanishes at zero momentum. The coupling becomes significant only when the momentum of the fermion becomes large. Because of this feature, the pseudoscalar coupling cannot overcome the dominant attractive, scalar exchange force if the constituents are not ultrarelativistic. Therefore the inclusion of the effective longitudinal Z^0 will not change our qualitative conclusions in any significant way in the intermediate-coupling region.

ACKNOWLEDGMENTS

B.L.Y. would like to thank C. P. Yuan for helpful discussions. P.J. and D.M. thank H. Munczek and J. Ralston for useful discussions and Lesley Smith for bringing Refs. [5–10] to our attention. This work was performed in part at Ames Laboratory under Contract No. W-7405-Eng-82 with the U.S. Department of Energy and was supported in part by the U.S. Department of Energy Grants Nos. DE-FG02-85ER40214 and DE-FG02-87ER40371, Division of High Energy and Nuclear Physics. One of the authors (A.J.S.) acknowledges financial support from a grant to Iowa State University from the U.S. Department of Education, Graduate Assistance in Areas of National Need Program.

APPENDIX A: BETHE-SALPETER CALCULATION

1. Bethe-Salpeter equation

We work with the standard Bethe-Salpeter amplitude [16]

$$\chi_p(x)=\langle 0|T[\psi(0)\bar{\psi}(x)]|p\rangle , \tag{A1}$$

where $|p\rangle$ is a color-singlet state of four-momentum p. Spinor and color indices are suppressed in our discussion. In order to establish notation and to provide the framework necessary to discuss approximations that we use, we sketch the derivation of the approximated form of our Bethe-Salpeter equations for a quark-antiquark system.

The general form of the homogeneous Bethe-Salpeter equation is, in momentum space,

$$\left[\frac{\not p}{2}+\not q-m\right]\chi\left[\frac{\not p}{2}-\not q+m\right]=V\chi , \tag{A2}$$

where m designates the fermion mass. This form is appropriate to the quark-antiquark channel in which we are interested.

Since we are primarily interested in heavy-quark-anticipated ($Q\bar{Q}$) systems with quark masses m_Q of order 100 GeV or more, we confine our discussion to the Coulombic part of the QCD potential. In the one-particle-exchange, or ladder, approximation to the "potential" V we have included the Higgs potential as well:

$$V\chi_p=-i\frac{g_Y^2}{4\pi}\int\frac{d^4q'}{4\pi^3}\chi_p(q')\frac{1}{(q-q')^2-M_H^2}$$
$$+i\int\frac{d^4q'}{4\pi^3}\frac{(\frac{4}{3}\alpha_s)}{(q-q')^2}\gamma_\mu\chi_p(q')\gamma^\mu , \tag{A3}$$

and $\frac{4}{3}\alpha_s$ is the QCD "fine structure constant" with the color-singlet factor $\frac{4}{3}$.

2. Salpeter's instantaneous approximation

To project onto a quarkonium state of definite spin-parity, one needs the matrix elements of Eq. (A2) between spinors $\bar{u}$ and v. Since $v=C(\bar{u})^T$ up to a phase, it is convenient to multiply Eq. (A2) on the right with the charge conjugation matrix C and recast Eq. (A2) in the form [16], restricting ourselves to 1^- exchange for this discussion:

$$\left[\frac{\not p}{2}+\not q-m\right]_1\left[\frac{\not p}{2}-\not q-m\right]_2 K$$
$$=\frac{i}{4\pi^3}\int\frac{d^4q'}{(q-q')^{'2}}\frac{4}{3}\alpha_s[(q-q')^2](\gamma_1)_\mu(\gamma_2)^\mu K(q')\ , \tag{A4}$$

where $K_{\alpha\beta}\equiv C_{\beta\beta'}\chi_{\alpha\beta'}$; the labels 1 and 2 distinguish the Q and $\bar{Q}$ variables. For lightly bound, Coulombic systems, one expects that $q^0-q_0'\ll m$ for the important contributions to the integral, and so we adopt a version of the "instantaneous" approximation, setting $(q-q')^2=-(\mathbf{q}-\mathbf{q}')^2$ in the denominator. Before collapsing takes place, E_B is of the order of 3–10 GeV in most of the cases investigated. Hence $|\mathbf{q}-\mathbf{q}'|$ is of the order of a few GeV which will be the energy scale that defines the QCD coupling, not the fermion mass as one might expect at first sight. This much smaller energy scale that is being exchanged between the fermion and antifermion as they propagate through the ladder also implies that the fermions and antifermions are mostly on mass shell. This is the reason why we choose the fixed value for the QCD coupling constant, $\frac{4}{3}\alpha_{\rm QCD}=0.25$. This value is also in accord with the estimates of the strong coupling given by Strassler and Peskin [10] (the strong interaction coupling constant is called $\alpha_{\rm eff}$ by the authors), who show a range of $\frac{4}{3}\alpha_{\rm QCD}$ between 0.28 and 0.21 for $100\le m_{\rm top}\le 500$. However, near collapsing, the momentum q and q' can be large and the value of $\alpha_{\rm QCD}$ will become smaller.

A similar discussion can be given to the Yukawa coupling, but here the effect of large Yukawa coupling has to be considered and the assumption of ladder dominance of the Bethe-Salpeter equation needs to be examined more carefully. One can imagine that in a more refined calculation, higher-order diagrams will be included. Parts of the high-order corrections due to vertex and propagator correction will turn the fixed coupling into a running coupling [27]. However, in the region away from the collapsing as argued in the paragraph above, the effect of the momentum dependence is not large since the high-order correction is only logarithmic and the range of momentum variation is small. Therefore a fixed value for g_Y would be a good approximation. However, the value of the coupling which has to be defined at some fixed point as an initial condition may be ambiguous. In the present application we interpret the value $g_Y=m_f/v$ to be defined with on-shell fermions and zero-momentum Higgs boson. Hence away from the collapsing point, g_Y will approximately be constant. Near collapsing, however, the wave function acquires large momentum components and variations in the Yukawa coupling may become significant. The reason is that the large initial Yukawa coupling means that the Landau pole [28,29] may not be too far away from the momentum range that is reachable in the problem under consideration as hinted from the one-loop result [27]. Then the Yukawa coupling can increase drastically. This will accelerate the collapsing so that the collapsing may occur earlier than Fig. 2 indicates.

In the approximation just described, the q_0' integral is simply

$$\int dq_0' K(q_0',\mathbf{q}')\equiv\chi(\mathbf{q}')\ ,$$

and one can recast the problem into the form of an integral equation for $\chi(\mathbf{q})$. Multiplying Eq. (A4) by

$$\left[\left[\frac{\not p}{2}+\not q-m\right]_1\left[\frac{\not p}{2}-\not q-m\right]_2\right]^{-1}$$

and integrating over q_0, one obtains, in the overall rest system $p=(E,\mathbf{0})$, a set of coupled homogeneous equations known as Salpeter's equations [14,15]:

$$(2\omega-E)\chi^{++}(\mathbf{q})=\Lambda_1^+(\mathbf{q})\Lambda_2^+(-\mathbf{q})\frac{4\alpha_s/3}{2\pi^2}\times\int\frac{d^3q'}{(\mathbf{q}-\mathbf{q}')^2}(1_1 1_2-\boldsymbol{\alpha}_1\cdot\boldsymbol{\alpha}_2)\times[\chi^{++}(\mathbf{q}')+\chi^{--}(\mathbf{q}')]\ , \tag{A5a}$$

and

$$(2\omega+E)\chi^{--}(\mathbf{q})=\Lambda_1^-(\mathbf{q})\Lambda_2^-(-\mathbf{q})\frac{4\alpha_s/3}{2\pi^2}\times\int\frac{d^3q'}{(\mathbf{q}-\mathbf{q}')^2}(1_1 1_2-\boldsymbol{\alpha}_1\cdot\boldsymbol{\alpha}_2)\times[\chi^{++}(\mathbf{q}')+\chi^{--}(\mathbf{q}')]\ , \tag{A5b}$$

where

$$\chi^{\pm\pm}(\mathbf{q})=\Lambda_1^{\pm}(\mathbf{q})\Lambda_2^{\pm}(-\mathbf{q})\chi(\mathbf{q})\ ,$$
$$\Lambda^{\pm}(\mathbf{q})=[\omega\pm(\boldsymbol{\alpha}\cdot\mathbf{q}+\beta m)]/2\omega\ .$$

Here $\omega=\sqrt{\mathbf{q}^2+m^2}$, $\boldsymbol{\alpha}=\gamma_0\boldsymbol{\gamma}$, and $\beta=\gamma_0$ in terms of the usual Dirac matrix convention. One also finds

$$\chi^{+-}(\mathbf{q})=\chi^{-+}(\mathbf{q})=0\ . \tag{A5c}$$

Our aim is to solve for the eigenvalues E in the individual spin-parity channels. To project Eqs. (A5a) and (A5b) into the appropriate channels, we first project onto the helicity basis, from combinations of definite total spin and finally project out amplitudes of definite total angular momentum J [30]. Designating helicity states in the total rest frame as $|\lambda_1,\lambda_2;\mathbf{q}\rangle$, we write the corresponding projections of Eqs. (A5a) and (A5b) as

$$(2\omega-E)\langle\lambda_1,\lambda_2;\mathbf{q}|\chi^{++}(\mathbf{q})\rangle=\frac{4\alpha_s/3}{2\pi^2}\langle\lambda_1,\lambda_2;\mathbf{q}|\Lambda_1^+(\mathbf{q})\Lambda_2^+(-\mathbf{q})\int\frac{d^3q'}{(\mathbf{q}-\mathbf{q}')^2}\sum_{h_1,h_2}(1_1 1_2-\boldsymbol{\alpha}_1\cdot\boldsymbol{\alpha}_2)|h_1,h_2;\mathbf{q}'\rangle$$
$$\times\langle h_1,h_2;\mathbf{q}'[|\chi^{++}(\mathbf{q}')\rangle+|\chi^{--}(\mathbf{q}')\rangle]\ , \tag{A6a}$$

$$(2\omega+E)\langle\lambda_1,\lambda_2;\mathbf{q}|\chi^{--}(\mathbf{q})\rangle=\frac{4\alpha_s/3}{2\pi^2}\langle\lambda_1,\lambda_2;\mathbf{q}|\Lambda_1^-(\mathbf{q})\Lambda_2^-(-\mathbf{q})\int\frac{d^3q'}{(\mathbf{q}-\mathbf{q}')^2}\sum_{h_1,h_2}(1_1 1_2-\boldsymbol{\alpha}_1\cdot\boldsymbol{\alpha}_2)|h_1,h_2;\mathbf{q}'\rangle$$

$$\times\langle h_1,h_2;\mathbf{q}'[|\chi^{++}(\mathbf{q}')\rangle+|\chi^{--}(\mathbf{q}')\rangle]\ , \tag{A6b}$$

where $\sum_{h_1,h_2}$ includes an energy sum over + and − energy solutions.

Now one uses the features of the energy projection operator:

$$\Lambda^+(\mathbf{q})u_\lambda(q)=u_\lambda(q)\ ,$$
$$\Lambda^-(\mathbf{q})v_\lambda(-\mathbf{q})=v_\lambda(q)\ , \tag{A7}$$

where

$$u_\lambda(\mathbf{q})=\left[\frac{\epsilon}{2\omega}\right]^{1/2}\begin{bmatrix}1\\ \dfrac{2\lambda|\mathbf{q}|}{\epsilon}\end{bmatrix}\chi_\lambda$$

and

$$v_\lambda(\mathbf{q})=\left[\frac{\epsilon}{2\omega}\right]^{1/2}\begin{bmatrix}\dfrac{2\lambda|\mathbf{q}|}{\epsilon}\\ 1\end{bmatrix}\bar{\chi}_\lambda$$

are the noncovariantly normalized spinors:

$$\sum_\lambda u_\lambda(\mathbf{q})u_\lambda^+(\mathbf{q})+\sum_\lambda v_\lambda(\mathbf{q})v_\lambda^+(-\mathbf{q})=1\ . \tag{A8}$$

The conventions in Eq. (A7) are

$$\omega=\sqrt{\mathbf{q}^2+m^2}\ ,$$
$$\epsilon=\omega+m\ ,$$
$$\chi_\uparrow=\begin{bmatrix}1\\0\end{bmatrix},\quad \chi_\downarrow=\begin{bmatrix}0\\1\end{bmatrix}, \tag{A9}$$
$$\bar{\chi}_\uparrow=\begin{bmatrix}0\\1\end{bmatrix},\quad \bar{\chi}_\downarrow=\begin{bmatrix}-1\\0\end{bmatrix}.$$

Following the notation of Ref. [14], we define

$$\chi_\lambda(\mathbf{q})=e^{-i\sigma_y(\theta/2)}\chi_\lambda(0)\ ,$$
$$\chi_\lambda(-\mathbf{q})=e^{-i\sigma_y(\theta/2)}\chi_{-\lambda}(0)\ ,$$

where $\mathbf{q}(-\mathbf{q})$ lies in the $x-z$ plane at an angle $\theta(\pi+\theta)$ with respect to the z axis.

From the helicity projections one forms the amplitudes of definite total spin.

(i) Spin singlet

$${}^0\chi(\mathbf{q})=\frac{\langle+,+;\mathbf{q}|\chi(\mathbf{q})\rangle-\langle-,-;\mathbf{q}|\chi(\mathbf{q})\rangle}{\sqrt{2}}\ . \tag{A10a}$$

(ii) Spin triplet

$${}^1\chi(\mathbf{q})=\frac{\langle-,+;\mathbf{q}|\chi(\mathbf{q})\rangle-\langle+,-;\mathbf{q}|\chi(\mathbf{q})\rangle}{\sqrt{2}}\ , \tag{A10b}$$

$${}^{12}\chi(\mathbf{q})=\langle+,+;\mathbf{q}|\chi(\mathbf{q})\rangle+\langle-,-;\mathbf{q}|\chi(\mathbf{q})\rangle\ , \tag{A10c}$$

$${}^{34}\chi(\mathbf{q})=\langle+,-;\mathbf{q}|\chi(\mathbf{q})\rangle+\langle-,+;\mathbf{q}|\chi(\mathbf{q})\rangle\ . \tag{A10d}$$

One obtains the total angular momentum projections by inverting the expansion of the interaction, $V\sim(\mathbf{q}')^{-2}$, in terms of the "rotating top" functions $d^J_{M,M'}(\theta)$:

$$\langle\lambda_1\lambda_2|V^J(q,q')|h_1h_2\rangle$$
$$=2\pi\int_{-1}^{+1}d(\cos\theta)d^J_{M,M'}(\theta)\langle\mathbf{q}\lambda_1\lambda_2|V|\mathbf{q}'h_1h_2\rangle\ ,$$

where $q=|\mathbf{q}|$, $M=\lambda_1-\lambda_2$, and $M'=h_1-h_2$. Integrals such as

$$\int d\Omega'(\mathbf{q}-\mathbf{q}')^{-2}P_J(\theta')=\frac{2\pi}{qq'}Q_J(Z)\ ,$$

where the $P_J(\theta)$ are the Legendre polynomials and the $Q_J(Z)$ are the Legendre functions of the second kind with $Z=(q^2+q'^2)/2qq'$ are used to express the equations in a form suitable for numerical solution.

The spin-0 equations are relatively compact, and they read

$$(2\omega-E)\,{}^0\chi_+^J(q)=\frac{4\alpha_s/3}{\pi}\frac{1}{q}\int_0^\infty dq'q'Q_J(Z)\left[\frac{2\omega\omega'-m^2}{\omega\omega'}\,{}^0\chi_+^J(q')+\frac{2\omega\omega'+m^2}{\omega\omega'}\,{}^0\chi_-^J(q')\right],$$
$$(2\omega+E)\,{}^0\chi_-^J(q)=\frac{4\alpha_s/3}{\pi}\frac{1}{q}\int_0^\infty dq'q'Q_J(Z)\left[\frac{2\omega\omega'+m^2}{\omega\omega'}\,{}^0\chi_+^J(q')+\frac{2\omega\omega'-m^2}{\omega\omega'}\,{}^0\chi_-^J(q')\right]. \tag{A11}$$

Equations (A11) are handled numerically by expressing the amplitudes as linear combinations of cubic B-splines and solving the resulting matrix equations by a Galerkin method using the Iowa State University (ISU) bound-state code [31].

Note that in each equation the opposite frequency amplitude is the more heavily weighted. This is especially clear when only the leading powers in q/m are kept in the integrand, and the expressions in square brackets become ${}^0\chi_+^J+3\,{}^0\chi_-^J$ and $3\,{}^0\chi_-^J+{}^0\chi_+^J$ in the ${}^0\chi_+^J$ and ${}^0\chi_-^J$ equations, respectively. This enhancement of the opposite energy contribution is due to the off-diagonal $\boldsymbol{\alpha}_1\cdot\boldsymbol{\alpha}_2$ part of the vector boson interaction. Interestingly, there is no such large

enhancement of opposite energy contributions from the $\alpha_1\cdot\alpha_2$ term in other partial waves.

3. The Blankenbecler-Sugar reduction of the Bethe-Salpeter equation

The Blankenbecler-Sugar equation [32] is one of an infinite set of so-called quasipotential equations which are three-dimensional reductions of the Bethe-Salpeter equation. The equation is obtained by replacing the center-of-momentum fermion propagator

$$\left[\left[\frac{\not p}{2}+\not q-m+i\epsilon\right]_1\left[\frac{\not p}{2}-\not q-m+i\epsilon\right]_2\right]^{-1}$$

by [33]

$$2\pi i\frac{m^2\Lambda_1^+(\mathbf{q})\Lambda_2^+(-\mathbf{q})}{\omega\left[\left[\frac{p}{2}\right]^2-\omega^2+i\epsilon\right]}\delta(q^0)=2\pi i\frac{m^2\Lambda_1^+(\mathbf{q})\Lambda_2^+(-\mathbf{q})}{\omega(\mathbf{k}^2-\mathbf{q}^2+i\epsilon)}\delta(q^0)\ , \tag{A12}$$

where $\mathbf{k}^2\equiv(p/2)^2-m^2=(E/2)^2-m^2$.

The δ function accomplishes the reduction to three dimensions. Carrying out an expansion in a helicity state basis yields, for the reduced Bethe-Salpeter equation [33],

$$\langle\mathbf{q}\lambda_1\lambda_2|\chi\rangle=\frac{m}{\mathbf{k}^2-\mathbf{q}^2}\sum_{h_1,h_2}\int d^3q'\langle\mathbf{q}\lambda_1\lambda_2|V|\mathbf{q}'h_1h_2\rangle\langle\mathbf{q}'h_1h_2|\chi\rangle\ . \tag{A13}$$

The partial wave decomposition is done as in Appendix A 1 with $E-2\omega$ replaced by $k^2/m-q^2/m$ and gives, for the spin-0 equation,

$$\left[\frac{q^2}{m}-B\right]{}^0\bar\chi_+^J(q)=\frac{4\alpha_s/3}{\pi}\frac{1}{q}\int_0^\infty dq'q'Q_J(Z)\left[\frac{2\omega\omega'-m^2}{m\sqrt{\omega\omega'}}{}^0\bar\chi_+^J(q')\right]\ , \tag{A14}$$

where B is the binding energy. The ${}^0\bar\chi_+^J(q)$ of Eq. (A14) is not the same function as the ${}^0\chi_+^J(q)$ of Eqs. (A11). Equation (A14) is solved using the ISU bound-state code [31].

4. Feynman gauge, covariant Bethe-Salpeter calculations

In the present paper we concentrate on the ground-state 0^- particles. For the pseudoscalar mesons χ can be decomposed as

$$\chi_P(p,q)=\gamma_5(\chi_0+\not p\chi_1+\not q\chi_2+[\not q,\not p]\chi_3)\ . \tag{A15}$$

In the weak binding limit, χ_0 and χ_1 dominate over the remaining functions and it is possible to solve Eq. (A2) quite accurately by keeping just these two functions. It is well known that the ladder approximated BS equation does not accurately reproduce the positronium spectrum though the correct $0^-,1^-$ splitting is obtained to leading order [21]. It is, however, suitable for the present study since we are not interested in obtaining the precise values of the binding energies but only to extract some qualitative features of how the binding energy changes as the coupling is increased.

For the deep-binding case, χ_0 dominates over all other functions and (A2) can be solved accurately by including only this function. Again the reliability of the ladder approximation is questionable when the coupling gets too large. However, our use of (A2) is not unreasonable since we are using it only to determine the value of the coupling at which the binding energy gets very large and where the ladder approximation breaks down completely. As discussed in the text, our results show a rather definite value of the coupling at which the mass of the pseudoscalar ground state suddenly drops to zero.

From the above discussion, it is clear that Eq. (A2) can be accurately solved in both the weak-coupling and strong-coupling (for bound-state mass $\simeq 0$) regime by including only the function χ_0 and χ_1. For the weak-coupling case it can be easily seen that

$$\chi_1=-\frac{\chi_0}{2m}\ .$$

Using this we find from (A2)

$$\chi_0=\frac{4}{3\pi^3}\frac{\alpha_s(q^2+m^2)}{D(q^2,M_B^2,\cos\theta)}\int d^4k\frac{\chi_0}{(k-q)^2}+\frac{g_Y^2}{D(q^2,M_B^2,\cos\theta)}\left[q^2+\frac{3M_B^2}{4}+m^2\right]\int\frac{d^4k}{(2\pi)^4}\frac{\chi_0}{(k-q)^2+M_H^2}\ , \tag{A16}$$

where $M_B^2=-p^2$ is the mass squared of the bound state, θ is the angle between p and q, and

$$D(q^2,M_B^2,\cos\theta)=\left[-q^2+\frac{M_B^2}{4}-m^2\right]^2+M_B^2q^2\cos^2\theta \ .$$

Equation (A16) has been written in terms of Euclidean variables. We reiterate that this equation also gives the correct limit of Eq. (A2) for the case when $M_B\to 0$, in addition to being reliable in the weak-coupling limit.

Equation (A16) is still quite complicated because of the dependence on the angle θ between p and q. In the pure QCD case, i.e., when $g_Y=0$, it is possible [16] to make a change of variables such that the resulting equation does not depend on this extra degree of freedom. In the general case, however, one has to find an approximation scheme to treat the two variable problems. In order to solve Eq. (A16) we will expand the ground-state wave function $\chi_0(q^2,M_B^2,\cos\theta)$ in terms of Tschebeshev polynomials $T^{(n)}(\cos\theta)$ [34]:

$$\chi_0(q^2,M_B^2,\cos\theta)=\sum_n \chi_0^{(n)}(q^2,M_B^2)T^{(n)}(\cos\theta) \ .$$

For the present paper, we will ignore all Tschebeshev polynomials higher than $T^{(2)}(\cos\theta)$. This approximation was found to be quite accurate for the present purpose since $T^{(2)}(\cos\theta)$ gave smaller than 15% correction to the binding energy for all the cases. The properly normalized $T^{(0)}$ and $T^{(2)}$ are given by

$$T^{(0)}(\cos\theta)=\left[\frac{2}{\pi}\right]^{1/2}, \quad T^{(2)}(\cos\theta)=\left[\frac{2}{\pi}\right]^{1/2}(4\cos^2\theta-1)$$

with the normalization

$$\int_0^\pi d\theta \sin^2\theta T^{(n)}(\cos\theta)T^{(m)}(\cos\theta)=\delta_{nm} \ .$$

$T^{(1)}$ does not give any contribution for the equal mass case. The equations for $\chi_0^{(0)}$ and $\chi_0^{(2)}$ can easily be obtained from Eq. (A2) by projecting out with appropriate $T^{(n)}$. We expect $\chi_0^{(0)}$ to be dominant for the ground state and therefore we can approximate $\chi_0^{(2)}$ by its inhomogeneous piece. We find

$$\chi_0^{(0)}=\frac{4}{3\pi^3}\alpha_s(q^2+m^2)\left[A_0\int d^4k\frac{\chi_0^{(0)}}{k-q^2}-\frac{A_2}{3}\int d^4k\frac{\chi_0^{(2)}}{(k-q)^2}\left[1-\frac{4(k\cdot q)^2}{k^2q^2}\right]\right]$$

$$+g_Y^2\left[q^2+\frac{3M_B^2}{4}+m^2\right]\left[A_0\int\frac{d^4k}{(2\pi)^4}\frac{\chi_0^{(0)}}{(k-q)^2+M_H^2}-\frac{A_2}{3}\int\frac{d^4k}{(2\pi)^4}\frac{\chi_0^{(2)}}{(k-q)^2+M_H^2}\left[1-\frac{4(k\cdot q)^2}{k^2q^2}\right]\right], \tag{A17}$$

$$\chi_0^{(2)}=\frac{A_2}{A_0}\chi_0^{(0)} \ ,$$

when A_0 and A_2 are given by

$$A_0=\frac{2}{C+\sqrt{C^2+M_B^2q^2C}} \ ,$$

$$A_2=\frac{-M_B^2q^2}{\left[C+\frac{M_B^2q^2}{2}+\sqrt{C^2+M_B^2q^2C}\right]\left[C+\sqrt{C^2+M_B^2q^2C}\right]} \ ,$$

$$C=\left[q^2-\frac{M_B^2}{4}+m^2\right]^2 \ .$$

For the ground state $\chi_0^{(0)}$ is a function only of q^2 and hence the angular integration in Eq. (A17) can be easily performed. The necessary integrals are given by

$$\int_0^\pi d\beta\frac{\sin^2\beta}{k^2+q^2+M_H^2-2|k||q|\cos\beta}=\frac{\pi}{k^2+q^2+M_H^2+[(k^2+q^2+M_H^2)^2-4k^2q^2]^{1/2}} \ ,$$

$$\int_0^\pi d\beta\frac{\sin^2\beta}{k^2+q^2+M_H^2-2|k||q|\cos\beta}(1-4\cos^2\beta)=-\pi\frac{4k^2q^2}{\{(k^2+q^2+M_H^2)+[(k^2+q^2+M_H^2)^2-4q^2k^2]^{1/2}\}^3} \ .$$

The resulting equations were then solved numerically. The results are given in Sec. II and III.

For the case of the vector mesons, since we are only interested in qualitative results, we simply use the well-known results in the weak-coupling and in the strong-coupling ($M_B=0$) case. In the weak-coupling case the vector-meson bound-state mass is slightly larger than the pseudoscalar meson mass, and the approximate splitting can be easily calculated by using the well-known nonrelativistic expansion. The strong-coupling ($M_B=0$) case for a pure Coulomb interaction is reviewed in Ref. [13]. One finds that the vector-meson mass becomes zero when the coupling $\alpha=2\pi$. Correspondingly the pseudoscalar meson mass for pure Coulomb interaction is zero for $\alpha=\pi/4$. This suggests that the vector-meson mass goes to zero much more slowly in comparison to the pseudoscalar meson mass as the coupling is increased. We expect similar behavior in the case of Higgs-boson exchange.

APPENDIX B: N/D METHOD

Here we summarize the N/D partial wave amplitude calculation of the ground-state mass with a Higgs-boson exchange in the t channel. For the fermion-antifermion partial-wave amplitude $T^J(s)$, where s is the invariant mass squared, one defines

$$[T^J(s)]_{\mu'\mu}\equiv\left[\frac{N^J(s)}{D^J(s)}\right]_{\mu'\mu}, \tag{B1}$$

where μ' and μ are final state and initial state helicities. $N^J(s)$ has only left-hand singularities and $D^J(s)$ has only right-hand singularities in the complex s plane [35]. Subtracting at $s=s_0$, one has

$$[D^J(s)]_{\mu'\mu}=1-\frac{s-s_0}{\pi}\int_{4m_f^2}^{\infty}\frac{[N^J(s')]_{\mu'\mu}}{(s'-s)(s'-s_0)}\rho(s')ds', \tag{B2}$$

where $\rho(s')=\frac{1}{2}\pi k(s')/\sqrt{s'}$ and $k(s')=\frac{1}{2}\sqrt{s'-4m_f^2}$ for two-body fermion-antifermion channel. We approximate $N^J_{\mu'\mu}$ by the one-Higgs-boson exchange amplitude (i.e., Born approximation, denoted T_B):

$$[N^J(s)]_{\mu'\mu}\approx[T_B^J(s)]_{\mu'\mu}=\frac{1}{2}\int_{-1}^{1}dx\, d^J_{\mu\mu'}(x)[T_B(x,s)]_{\mu'\mu}, \tag{B3}$$

with x the cosine of the scattering angle in the center of mass. In more detail, we write $T_B(x,s)_{\mu'\mu}\equiv T_B(x,s)^{\lambda_2',\lambda_1';\lambda_1\lambda_2}$,

$$[T_B(x,s)]^{\lambda_2',\lambda_1';\lambda_1\lambda_2}=-\frac{g_Y^2\bar{u}(p_1',\lambda_1')u(p_1,\lambda_1)\bar{v}(p_2,\lambda_2)v(p_2',\lambda_2')}{M_H^2+(s-4m_f^2)^{1/2}(1-x)}, \tag{B4}$$

where $\mu'=\lambda_1'-\lambda_2'$, $\mu=\lambda_1-\lambda_2$, and $s=(p_1+p_2)^2=(p_1'+p_2')^2$. The spinors and antispinors are u and v and spinor indices are suppressed, as usual. The Yukawa coupling of the Higgs boson to the fermion is denoted by g_Y.

For the ground state with $J^P=0^-$ we need the spin-0, negative-parity and total angular momentum zero projection [35]. Defining

$$f\equiv T_{++;++}-T_{++;--}$$

and

$$f^J=\frac{1}{2}\int_{-1}^{1}f d^J_{00}(x)dx, \tag{B5}$$

from (B4) and (B5) we find that our Born approximation gives the 0^- amplitude

$$f^0(s)=\frac{g_Y^2}{4\pi^2}\left[1+\frac{4m_f^2-M_H^2}{4p^2}\ln\left[1+\frac{4p^2}{M_H^2}\right]\right], \tag{B6}$$

with the Born approximation understood and where p is the magnitude of the quark three-momentum in c.m. system. In the standard model, $g_Y=m_f/v$ where $v\simeq 250$ GeV, which is the value we will adopt for our numerical work.

The condition for the formation of a bound state is that the $D^J(s)$ function vanish for some value of s below threshold, $s_B\le 4m_f^2$, and referring back to (B2), we write

$$0=1-\frac{s_B-s^0}{\pi}\int_{4m_f^2}^{\infty}ds'\frac{\rho(s')f^0(s')}{(s'-s^0)(s'-s_B)}, \tag{B7}$$

$s_B<4m_t^2$, as our bound-state condition in this model. This condition assumes a rather simple form if we rescale p^2 by $4m_f^2$, use $y=p^2/4m_f^2$ as our variable, and define $R_B^2=s_B/4m_f^2$ and $R_0^2=s_0/4m_f^2$,

$$0=1-\frac{g_Y^2}{16\pi^2}[I(R_B^2)-I(R_0^2)], \tag{B8a}$$

where

$$I(R^2)=\int_0^{\infty}dy\frac{1}{[y(1+y)]^{1/2}}\frac{1}{y+1-R^2}\times\left[R^2-1+(1-R_H^2)\ln\left[1+\frac{y}{R_H^2}\right]\right] \tag{B8b}$$

and the bound-state mass value squared is given by

$$M_B^2=s_B=4m_f^2R_B^2.$$

[1] CDF Collaboration, F. Abe *et al.*, Phys. Rev. Lett. **68**, 447 (1992).
[2] P. Langacker and M. Luo, Phys. Rev. D **44**, 817 (1991).
[3] M. Chanowitz, M. Furman, and I. Hinchliffe, Nucl. Phys. **B153**, 402 (1979).
[4] M. Veltman, Nucl. Phys. **B123**, 89 (1977); P. Q. Hung, Phys. Rev. Lett. **42**, 873 (1979); H. Politzer and S. Wolfram, Phys. Lett. **82B**, 242 (1979); **83B**, 421(E) (1979).

[5] H. Inazawa and T. Morii, Phys. Lett. B **203**, 279 (1988).
[6] H. Inazawa and T. Morii, Z. Phys. C **42**, 563 (1989).
[7] H. Inazawa, T. Morii, and J. Morishita, Z. Phys. C **46**, 273 (1990).
[8] J. Feigenbaum, Phys. Rev. D **43**, 264 (1991).
[9] W. Kwong, Phys. Rev. D **43**, 1488 (1991).
[10] M. Strassler and M. Peskin, Phys. Rev. D **43**, 1500 (1991).
[11] V. S. Fadin and V. A. Khoze, Pis'ma Zh. Eksp. Teor. Fiz. **46**, 417 (1987) [JETP Lett. **46**, 525 (1987)].
[12] An early discussion on zero-mass bound states was given by J. S. Goldstone, Phys. Rev. **91**, 1516 (1953). For early references on this subject, see L. G. Suttorp, Nuovo Cimento **29A**, 225 (1975); **33A**, 257 (1976). For a recent review, see N. Seto, Prog. Theor. Phys. Suppl. **95**, 25 (1988).
[13] Seto [12].
[14] J. J. Kubis, Phys. Rev. D **6**, 547 (1972); K. Erkelenz, Phys. Rep. **13C**, 192 (1974); R. Machleidt, K. Holinde, and Ch. Elster, *ibid.* **179**, 1 (1987).
[15] E. Salpeter, Phys. Rev. **87**, 328 (1952).
[16] A review of the Bethe-Salpeter equation and its application to positronium is given by C. Itzykson and I. Zuber, *Quantum Field Theory* (McGraw-Hill, New York, 1980). We follow their notation.
[17] See, for example, Prog. Theor. Phys. Suppl. **95** (1988). Especially useful in this context is the review by T. Murota, *ibid.* **95**, 46 (1988).
[18] These order-α^2 and -α^4 results can be obtained in more than one way. For a Schrödinger-type perturbative treatment, see H. A. Bethe, *Quantum Mechanics of One- and Two-Electron Atoms* (Plenum, New York, 1977), Sec. 23. The same is obtained in the Bethe-Salpeter approach in Ref. [16], Sec. 10-3-2.
[19] H. W. Crater and P. Van Alstine, Phys. Rev. D **37**, 1982 (1988).
[20] S. Love, Ann. Phys. (N.Y.) **113**, 153 (1978).
[21] See also Murota [17] and the discussion in Itzykson and Zuber [16].
[22] Goldstone [12].
[23] R. W. Haymaker, Phys. Rev. D **13**, 968 (1976); **16**, 1211 (1977).
[24] P. Caussignac and G. Wanders, Nuovo Cimento **55A**, 45 (1980).
[25] G. Rupp, University of Maryland Report No. 92–131 (unpublished); another recent Higgs-boson bootstrap is presented by D. Sivers and J. Uretsky, Phys. Rev. Lett. **68**, 1649 (1992).
[26] In Rupp's calculation the kernel includes the ladder diagrams as well as the *s*-channel bubble diagrams. The *s*-channel bubble diagrams give rise to a repulsive force and can therefore slow down the collapsing as a function of the coupling constant. We have checked his result against that of the ladder diagrams alone. Indeed the inclusion of the *s*-channel bubble diagram postpones the collapsing (by a factor 2) as a function of the constituent scalar particle mass.
[27] T. P. Cheng, E. Eichten, and L. F. Li, Phys. Rev. D **9**, 2259 (1974); C. T. Hill, *ibid.* **24**, 691 (1981). We thank Professor Li for a discussion of the fermion–Higgs-boson running coupling.
[28] L. D. Landau, A. A. Abrikosov, and I. M. Khalatnikov, Dokl. Akad. Nauk SSSR **95**, 1177 (1954).
[29] The existence of a Landau pole in the nucleon–pseudoscalar-meson coupling was pointed out in A. D. Galanin, B. L. Ioffe, and I. Ia. Pomeranchuk, Zh. Eksp. Teor. Fiz. **29**, 51 (1956) [Sov. Phys. JETP **2**, 37 (1956)]. We thank Professor Ioffe for pointing this out to us.
[30] This procedure is reviewed by R. Machleidt, K. Holinde, and C. Elster, Phys. Rep. **147**, 1 (1987), for a variety of potentials under the further approximation $\chi^{--}=0$. See also K. Erkelenz, Phys. Rep. **13**, 191 (1974).
[31] J. Spence, Ph.D. thesis, Iowa State University, 1989.
[32] R. Blankenbecler and R. Sugar, Phys. Rev. **142**, 1051 (1966).
[33] This replacement is that proposed by M. Partovi and E. Lomon, Phys. Rev. D **9**, 1999 (1970), as a way to adapt the method of Ref. [32], which deals with scalar particles, to the spinor-spinor Bethe-Salpeter equation.
[34] P. Jain and H. Munczek, Phys. Rev. D **44**, 1873 (1991); **46**, 438 (1992).
[35] P. D. B. Collins and E. J. Squires, *Regge Poles in Particle Physics,* Springer Tracts in Modern Physics Vol. 45 (Springer, Berlin, 1968), Chap. VI. We use the notation of A. D. Martin and T. D. Spearman, *Elementary Particle Theory* (North-Holland, Amsterdam, 1970).